SAND REPORT
SAND2002-4178
Unlimited Release
Printed January 2003

A Novel Microcombustor for Sensor and Thermal Energy Management Applications in Microsystems

R. P. Manginell, M. W. Moorman, C. W. Colburn, L. F. Anderson, T. J. Gardner, D. L. Mowery-Evans, P. G. Clem, S. B. Margolis

Prepared by
Sandia National Laboratories
Albuquerque, New Mexico 87185 and Livermore, California 94550

Sandia is a multiprogram laboratory operated by Sandia Corporation, a Lockheed Martin Company, for the United States Department of Energy's National Nuclear Security Administration under Contract DE-AC04-94-AL85000.

Issued by Sandia National Laboratories, operated for the United States Department of Energy by Sandia Corporation.

Available to DOE and DOE contractors from
U.S. Department of Energy
Office of Scientific and Technical Information
P.O. Box 62
Oak Ridge, TN 37831

Telephone: (865)576-8401
Facsimile: (865)576-5728
E-Mail: reports@adonis.osti.gov
Online ordering: http://www.doe.gov/bridge

Available to the public from
U.S. Department of Commerce
National Technical Information Service
5285 Port Royal Rd
Springfield, VA 22161

Telephone: (800)553-6847
Facsimile: (703)605-6900
E-Mail: orders@ntis.fedworld.gov
Online order: http://www.ntis.gov/help/ordermethods.asp?loc=7-4-0#online

SAND2002-4178
Unlimited Release
Printed December 2002

A Novel Microcombustor for Sensor and Thermal Energy Management Applications in Microsystems

R. P. Manginell, M. W. Moorman, C. W. Colburn, L. F. Anderson
Micro-Total-Analytical Systems Department

T. J. Gardner
Ceramic and Glass Department

D. L. Mowery-Evans, P. G. Clem
Materials Chemistry Department

S. B. Margolis
Industrial and Combustion Processes Department

Sandia National Laboratories
P.O. Box 5800
Albuquerque, NM 87185-0603

Abstract

The microcombustor described in this report was developed primarily for thermal management in microsystems and as a platform for micro-scale flame ionization detectors (microFID). The microcombustor consists of a thin-film heater/thermal sensor patterned on a thin insulating membrane that is suspended from its edges over a silicon frame. This micromachined design has very low heat capacity and thermal conductivity and is an ideal platform for heating catalytic materials placed on its surface. Catalysts play an important role in this design since they provide a convenient surface-based method for flame ignition and stabilization. The free-standing platform used in the microcombustor mitigates large heat losses arising from large surface-to-volume ratios typical of the microdomain, and, together with the insulating platform, permit combustion on the microscale. Surface oxidation, flame ignition and flame stabilization have been demonstrated with this design for hydrogen and hydrocarbon fuels premixed with air. Unoptimized heat densities of 38 mW/mm^2 have been achieved for the purpose of heating microsystems. Importantly, the microcombustor design expands the limits of flammability (LoF) as compared with conventional diffusion flames; an unoptimized LoF of 1-32% for natural gas in air was demonstrated with the microcombustor, whereas conventionally 4-16% observed. The LoF for hydrogen, methane, propane and ethane are likewise expanded. This feature will permit the use of this technology in many portable applications were reduced temperatures, lean fuel/air

mixes or low gas flows are required. By coupling miniature electrodes and an electrometer circuit with the microcombustor, the first ever demonstration of a microFID utilizing premixed fuel and a catalytically-stabilized flame has been performed; the detection of ~1-3% of ethane in hydrogen/air is shown. This report describes work done to develop the microcombustor for microsystem heating and flame ionization detection and includes a description of modeling and simulation performed to understand the basic operation of this device. Ancillary research on the use of the microcombustor in calorimetric gas sensing is also described where appropriate

Acknowledgements

The authors would like to acknowledge Patrick R. Lewis and Richard J. Kottenstette for numerous discussions that lead to this project and extremely valuable technical assistance along the way. They would like to thank Linda McLaughlin for her assistance in catalyst preparation and Ronald Sandoval for his help in catalyst testing. They would also like to thank Sara S. Sokolowski, L. James Sanchez and Sherry Zmuda for fabrication, mechanical engineering support and SEMs, respectively. Sandia is a multiprogram laboratory operated by Sandia Corporation, a Lockheed Martin Company, for the United States Department of Energy under contract DE-AC04-94AL85000.

Table of Contents

Introduction

The development of a small and stable on-chip flame/combustor, or microcombustor, would permit the adaptation or translation of several very useful macroscopic devices into the microsystem domain: on-chip flame ionization detectors (microFIDs), microreactors, micropropulsion, energy conversion and, importantly, heating and thermal management. The argument for the use of on-chip combustive heating is compelling. The energy density of butane, including storage cylinder mass, is 50 times that of the best high-output batteries ($LiMnO_2$ nonrechargable). Thus, a tiny fuel tank could replace several bulky batteries in hand-held microanalytical systems like the μChemLab™, and would supply a microcombustor for efficient heating of essential components.

Stable flames are difficult to achieve on a small scale due to enhanced heat loss arising from large surface-to-volume ratios. Catalytic materials provide a natural, surface-based method for flame ignition and stabilization. The premise of this research was that by placing such materials on the surface of a miniature, electrically-heated, thermally-isolated membrane (microhotplate), further stabilization can be achieved; this combination of a microhotplate and catalyst materials for sustained combustion on the microscale is what is referred to as a microcombustor (Figure 1). Indeed, this research shows that this design not only permits stable flames in the microdomain, but the limits of flammability (LoF) are expanded as compared with diffusion flames. This, in turn, has important consequences for microanalytical systems: not only is the energy density of combustible gases relatively high, as mentioned above, but the microcombustor allows for lean burning at low flows and at temperatures less severe than with diffusion flames. These imply longer system lifetime and smaller fuel supplies, both of which are especially important for portable applications.

Other groups have used conceptually similar microcombustor designs to fashion micro chemical reactors for partial oxidation synthesis [1], power generation and hydrogen reforming [2] and gas sensing [3,4,5,6]. For the work described in this report, there were two main goals: demonstrate the use of microcombustors in (a) heating of microanalytical systems, and (b) in the construction of a microFID. Calorimetric gas sensing, closely related to application ‘a’, was investigated in a parallel research effort using the microcombustor; as appropriate, those results are presented here.

It is important to note that a flame ionization detector measures a current generated from hydrocarbon ionization to measure fuel carbon content. Using the microcombustor as a basis, the first ever demonstration of a microFID, utilizing lean premixed fuel and a catalytically-stabilized flame, is reported here. Importantly, the catalyst not only aids in combustion, but also apparently aids in reduced-temperature (relative to conventional flames) formation of hydrogen radicals, which are necessary for cracking of hydrocarbons into single carbon fragments. This step is a critical one in the overall FID mechanism [7]. MicroFID systems created by other groups [8] have used micromachined nozzles to anchor an oxyhydrogen diffusion flame; hydrogen flow rates on the order of 35 ml/min were required for flame stabilization in this design. Flame stabilization via catalytic surfaces in the present microcombustor permits stable combustion at hydrogen flows less than 5 ml/min and under lean conditions, although the microFID has not yet been demonstrated in this flow regime. Again, reduced fuel consumption and operation temperature are very important features of the microcombustor.

To supplement the experimental approach mentioned above and to understand and optimize microcombustor performance, modeling and simulation was undertaken. Fundamental studies

explained catalytic extension of LoF despite enhanced heat losses; these studies also showed the possibility of multiple stable operating points. Simulation in Aurora, a continuously-stirred reaction model, predicted average temperature increases and helped explain premature failure of the microcombustor under certain operating conditions. ANSYS modeling was used to predict the benefits of microcombustor heating of microsystems. The results of this modeling effort are summarized.

Figure 1: Left: Schematic cross section of the microcombustor. Center: Microhotplate used for the microcombustor (backlit). Right: Micropenned Pt/alumina, 25 μm thick, on the microhotplate.

Finally, reliable deposition of catalysts is very important for this type of device, and techniques such as slurry deposition [6] and chemical vapor deposition [4,5,9] have been used in the past. In this work, the list of commonly used catalyst deposition methods was extended by using a new micropen deposition technique to reliably, and uniformly, deposit the necessary catalysts. The micropen could control the placement of the catalyst, while precisely controlling the catalyst volume. Several different formulations of Pt and Pd based catalysts have been developed to allow micropen deposition onto the microhotplates. Supported catalysts as thin as 15 microns have been demonstrated with this technique. Catalyst performance was independently investigated by using a conventional u-tube combustion rig.

Microhotplate Fabrication

The microhotplate, used as a basis for the microcombustor, was fabricated by through-wafer silicon etching [9]. It consisted of a silicon nitride membrane suspended from a frame of Si (see Figure 1 and Figure 2). Either Bosch etching or KOH etching could be used to release the membrane, with no discernable operational differences between the completed devices made by either method. In the case of Bosch etching, an etch stop layer of 0.5 micron thermally-grown oxide was used to prevent undesired etching of the 1 micron thick low-stress silicon nitride membrane layer; any residual oxide remaining after the Bosch etch is stripped in buffered HF. For KOH etching, no additional etch stop layer was required. Prior to silicon etching by either method, a thin-film Ti/Pt heater was patterned on the membrane layer on the opposite side of the wafer from the etch window; typically, ~1700 Å of Pt and a 100 Å Ti adhesion layer were used. The heating elements double as temperature sensors by monitoring the resistance change of the wire caused by thermal fluctuations. Due to their thermal sensitivity, typically better than 0.4 mW/°C, microhotplates have been used in a number of other applications including flow sensing [10,11] gas thermal conductivity detection [12,13] infrared bolometry [14,15] and conductometric gas sensing [16], typically using tin oxide as a gas sensitive layer for the latter.

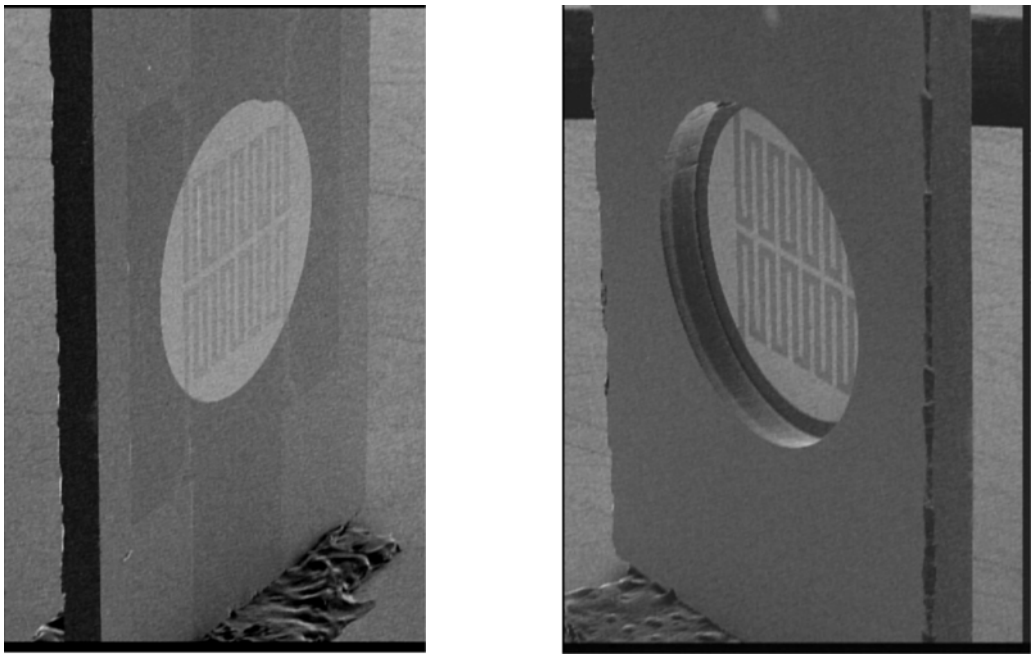

Figure 2: Left: Scanning electron micrograph (SEM) of the front, metalized surface of the microhotplate. The meandering heater is apparent, as is the circular shape of the suspended SiN membrane. Right: SEM of the back, etched side of the microhotplate. The heater is visible through the SiN and the circular etch pit is evident.

Cata[illegible]on

In order to utilize the microhotplate [illegible]e a suitable catalyst placed on its surface. In the initial stages of th[illegible]based microhotplate heater was actually used as the catalyst due to i[illegible]ering. Temperature sensor data indicated that the microcombustor [illegible]operation, resulting in premature failure. SEM images of the platinum[illegible]icate at least three failure modes: (1) agglomeration of the thin-film [illegible]the membrane such as pitting or rupturing, and (3) delamination of [illegible] membrane. These three failure modes are shown in Figure 3. Mo[illegible]revalent and is explained by the tendency of thin films to agglomera[illegible]ring at high temperature. Direct exposure of the thin-film metalizat[illegible]s would also result in long-term drift in heater resistance and cataly[illegible]ight device failures like those in Figure 3, did not occur.

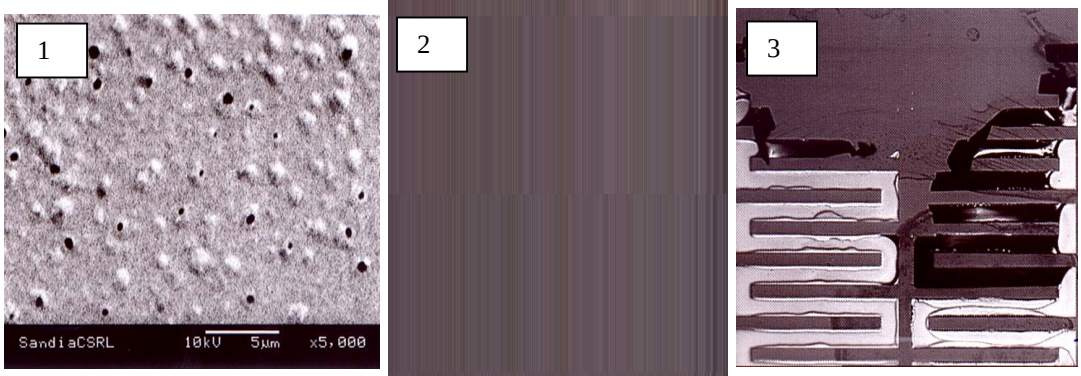

1500X 5X 5X

Figure 3: Various degrees of damage to the microhotplate metal after microcombustor experiments. SEM 1 (left) shows localized microstructural agglomeration of Pt and pitting. SEM 2 (center) shows a localized hot spot, which resulted in microhotplate device failure. SEM 3 (right) shows severe metal delamination from the underlying SiN membrane.

Preliminary work with thin-film catalysts motivated the transition to catalysts supported in high-temperature-stable, high-surface-area materials, such as alumina or hydrous titanium oxide (HTO). Note: with the exception of data taken with the U-tube reactor, below, where thin-film Pt, Pt/HTO and Pt/alumina catalysts were evaluated, all microcombustion and FID data presented in the remainder of the paper was taken using only alumina-supported catalysts. These catalysts not only showed enhanced stability and reactivity as compared with the thin films, they also helped to mitigate against the reliability problems and failure modes described above by insulating the thin-film heater elements from the harsh combustion conditions.

The supported catalysts used in the combustion and FID tests were from either a commercial supplier or from in-house-prepared catalysts. Both utilize noble metals supported in an alumina matrix. When compared with the commercial material, the in-house catalysts performed well. While all catalysts have proven capable of combusting hydrogen, methane, ethane, propane, and

natural gas, at higher flow rates the internally-developed Pt catalyst promotes more efficient combustion.

Initially, all catalysts were manually deposited by drop coating. While this process was acceptable for preliminary testing, it was too variable in terms of catalyst thickness and location for more advanced studies. In order to achieve repeatability, an Ωhmcraft Micropen 400 printing system was adapted for catalyst deposition. Three basic catalysts powders were prepared in house: pure alumina, 1 wt% Pt/alumina, and 1 wt% Pd/alumina. All materials were calcined for 2 hours at 600 °C in air and were prepared by incipient wetness. Pastes or "inks" suitable for direct-write printing with the micropen were then created from the powders. Both aqueous (water + additives) and organic solvent systems were used in paste production, though for the data presented here, only aqueous pastes were evaluated. For aqueous pastes, the powder catalysts were dispersed in water with a pH adjusted to ~ pH 4 using nitric acid. A drying inhibitor, Avecia Humectant GRB2, was added to prevent rapid evaporation, which would otherwise clog the pen tip between printing runs, and cause cracking of the deposited paste during drying. The alumina/water/GRB2 paste was mixed for 15 minutes in a Nalgene bottle using alumina media to reduce catalyst agglomerate size, using a Specs Mill. Reduction of agglomerate size is necessary to allow smooth paste flow through the Micropen tips, which are 25-250 μm in size. Pastes were partially dried or diluted with water, and milled again until the desired rheology was obtained. The final paste had a weak yield stress and resisted flow due to gravity but flowed easily under applied pressure, as in the micropen print conditions. Typical pastes were in the range of 10-30 volume percent solids.

The Micropen is a thick film direct write tool originally designed for precision value resistors, which write patterns by dispensing a controlled volume of slurry/paste through a pen tip onto a moving X-Y print table. For the catalyst layers, a print area was designed in AutoCAD to fit on the active area of a microhotplate, and transferred to a print file within the Micropen software package. A printed, 25 μm thickness Pt:Al_2O_3 catalyst pad is shown in Figure 4b. The thickness of the catalyst layers was designed to be in the range of 25-75 μm, in which range high reproducibility and good adhesion was obtained. The micropen dispenses a controllable volume of paste per time, which enables control of thickness by varying print volume, paste concentration, and write speed. Film thickness was characterized using a COBRA laser profilometer. Finally, printed catalyst pads were dried at 100-300ºC to enable solvent removal and were then ready for microcombustor testing. Figure 4 shows a hotplate before and after catalyst deposition.

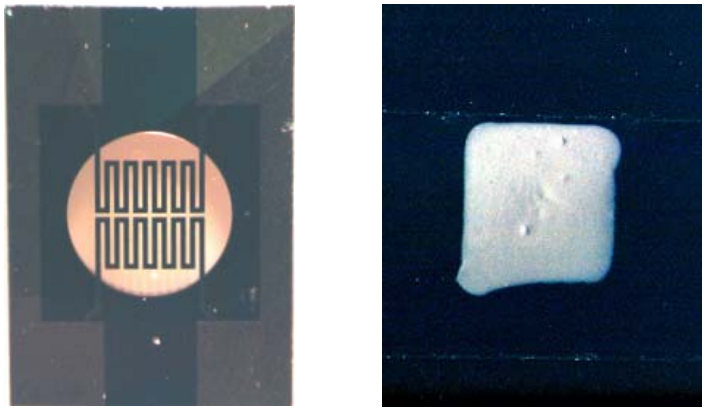

Figure 4: Left: Microhotplate used for the microcombustor (backlit). Right: Micropenned Pt/alumina, 25 μm thick, on the microhotplate.

Microcombustor Test Apparatus

Following catalyst deposition, device packaging was the next step in preparing a microcombustor. Initially, conventional ceramic DIPs were used, and electrical connections to the package were made via wire bonds. Subsequently, small, conventionally-machined, glass lids with gas inlets/outlets and a flow channel were affixed with epoxy onto the microcombustors (Figure 5). The application of the lids to the substrates was a difficult technical task, often causing membrane rupture. The small size and insulating properties of these lids meant that water vapor, produced during combustion, could condense in the interior of the fixture, making combustion difficult to maintain, and causing pressure fluctuations capable of rupturing the SiN membrane. While several experiments were performed with this packaging, it required time consuming assembly, with low yield, and was eventually abandoned for packaging schemes tailored to specific experimental needs.

U-tube reactor

To study catalyst behavior independent of the microcombustor in a well-characterized conventional apparatus, some catalyst testing was performed in a u-tube reactor. The u-tube had an internal diameter of 4 mm and the catalyst bed was held into place using quartz wool. The u-tube reactor was placed in a heating mantle and the temperature was monitored by a thermocouple placed at the top of the catalyst bed. Hydrogen conversion was measured using a TCD detector with argon as a carrier and reference gas. For transient temperature experiments, the temperature controller was programmed to ramp at 5 °C/min.

Drop-in microcombustor array test fixture

To address the issues with the glass lid, and permit drop-in replacement and testing of the microcombustor, a fixture with a larger internal volume was constructed. Figure 5 (Right) shows a schematic of the combustion fixture. The fixture, additionally, possessed all the necessary ports for gas flow, electrical interconnection, and temperature sensing. Internally, the fixture's volume was about 683 mm^3. The gas inlet, with an inner diameter of 315 microns, was placed about 1.5 mm above the microcombustor die, which assured that the gas stream would not directly impinge on the microhotplate. The fixture used conventional wiring, which could be manually soldered onto the microcombustor dies to accommodate various bond pad layouts. Overall, this reduced device preparation time significantly. The larger internal volume meant that water vapor was free to exit the fixture, instead of dousing the flame as it had previously, and that the membranes were no longer subjected to failure-inducing pressure loadings. The base plate of the fixture had the necessary space to mount two microcombustor devices. In this way different coatings could be tested simultaneously in an array concept. After catalyst deposition and fixturing was complete, the device could be tested.

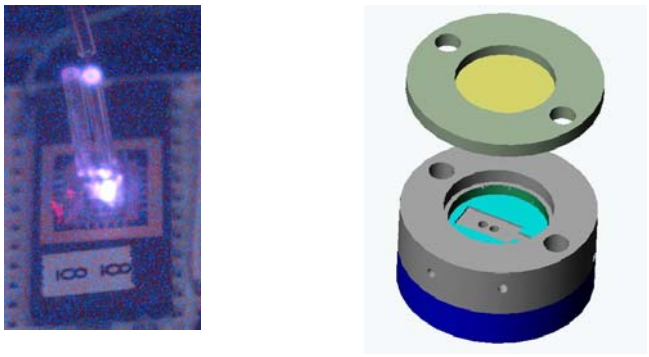

Figure 5: Left: Image of the microcombustor with glass lid and flame. Right: Schematic of the combustion fixture with upper lid removed and die inset revealed.

MicroFID fixture

For the FID experiments, the original ceramic packaging with glass lids mentioned above was temporarily resurrected. Since a large internal combustion volume would require an appropriately large potential for ion collection, it was decided to continue use of modified glass lids for the initial experiments. A small glass lid, with an inner cavity of approximately 2.5 mm diameter and 150 microns of height, was placed over the microhotplate membrane, and sealed with epoxy. The top of the glass lid had three holes for gas input, exhaust, and electrical connection to the lid electrode. A small planar nickel electrode, of approximately 2 mm diameter was embedded in the top of the lid to provide one of the requisite potential sources for ion collection. Capillary tubes, with a 315 micron inner diameter, were used for the gas input. Figure 6b shows a cross-sectional schematic of the prepared device during combustion (this configuration is substantially similar to the actual device shown in use in Figure 5a). A microcombustor, shown in Figure 6 (Left and Right)without catalyst for clarity, was drop coated with a layer of commercially-available platinum catalyst, and provided flame ignition and stabilization for the FID.

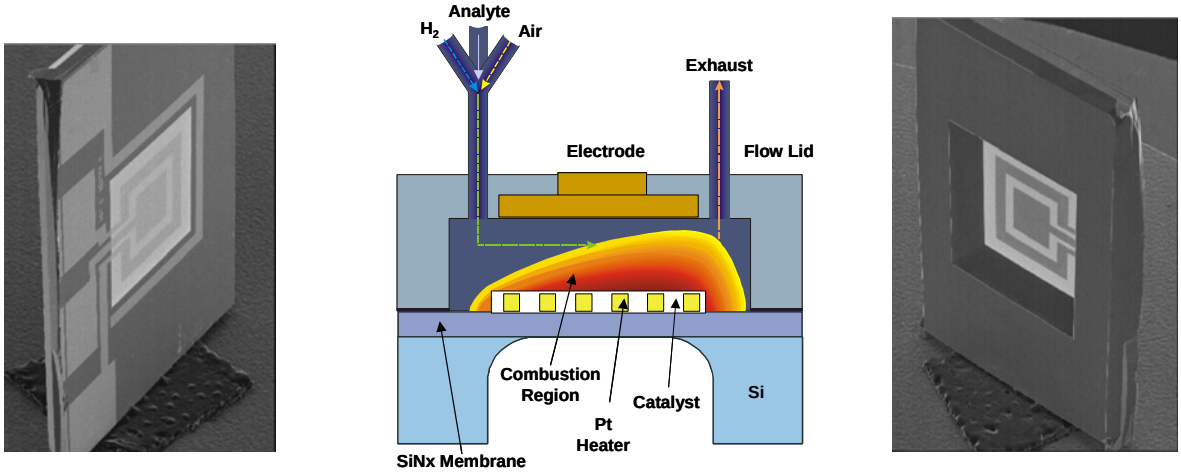

Figure 6: Left: SEM of microhotplate used in microFID, front side. Center: Cross-sectional schematic of microFID with lid. Right: SEM of microhotplate used in microFID, etch side.

U-Tube Reactor Catalyst Evaluation

To reiterate, the U-tube reactor was used to independently evaluate the behavior of several types of catalysts. In the first sub-section below, thin-film Pt catalysts, hydrous titanium oxide (HTO) supported catalysts, and a commercially-supplied Pt/alumina catalyst are discussed. The commercially-available Pt/alumina was used in the microFID experiments. The second sub-section briefly describes u-tube testing of micropenned, internally-developed Pt/alumina catalysts. This material is relevant to the microcombustor testing section. It is important to note that all microcombustion and FID data presented in the remainder of the paper, exclusive of this section, was taken using only alumina-supported catalysts.

Thin film Pt, HTO-supported Pt and commercial Pt/alumina catalysts

Electron-beam evaporated thin Pt films (150 nm) were prepared with either titanium or tantalum as an adhesion layer (10 nm) on a SiN-coated Si test piece. A supported catalyst was made with a hydrous titanium oxide-supported Pt (1% Pt-HTO) slurry spin-coated onto a 10 nm Ti layer deposited on a SiN-coated silicon die. For comparison, a commercial Pt/Al_2O_3 catalyst was also tested. Catalyst test pieces were crushed before being placed in the u-tube.

Unless otherwise indicated, catalysts were evaluated under dilute stoichiometric conditions (3.7% H_2, 1.9% O_2 and balance He and Ar). For most cases the total geometric surface area of the catalyst was 1 cm^2 and the total gas flow rate was 16 milliliters per minute (ml/min). In cases that the geometric surface area of the catalyst was not 1 cm^2, the total gas flow rate was adjusted proportionally; i.e., for a 0.5 cm^2 sample, the flow rate would be 8 sccm. Hydrogen conversion was measured as the temperature was ramped-up to 300 °C and back down to room temperature at 5 °C per minute. On the ramp-up, the temperature for 50% conversion (T_{50}) of H_2 was approximately 150 °C for all three samples, shown in Figure 7 (Left). Even on the ramp-up, the Pt/Ti film showed loss of activity after reaching 165 °C. On the subsequent ramp down, the Pt/Ti film lost almost all of its activity, while the Pt/Ta film showed significant deactivation with T_{50} increasing ~40 °C. However, the activity of the Pt/HTO catalyst increased as evidenced by the T_{50} decrease of ~35 °C after the ramp to 300 °C (see Figure 7b). No loss of activity was seen for the Pt/HTO even after ramping the temperature to 600 °C (not shown).

In a separate experiment, H_2 conversion as a function of time was measured at 150 °C for both Pt/Ta and Pt/Ti samples. Activity decreased significantly for both cases; in 20 minutes the Pt/Ti and Pt/Ta films lost greater than 90% and ~60% of their original activity, respectively (see Figure 8). Microstructural examination of the samples after the testing at 150°C showed damage similar to that shown in Figure 3 (Left). These results show that catalyst durability can be increased using Ta instead of Ti as a sticking layer, but larger gains in durability and enhanced activity can be achieved by switching to a supported catalyst.

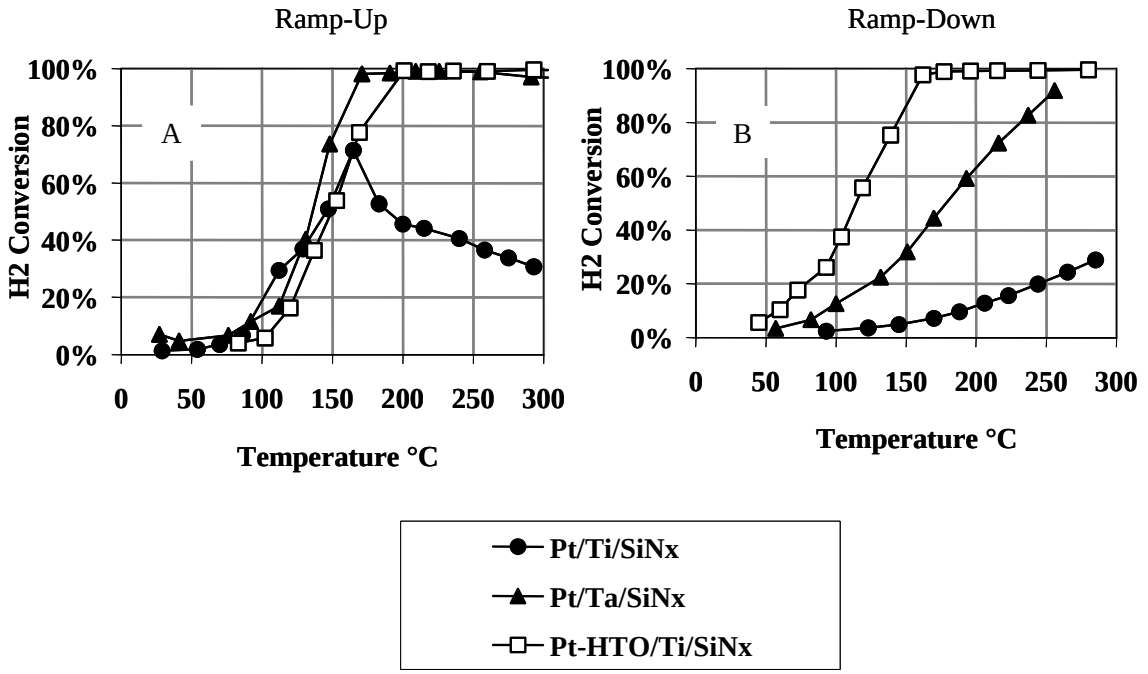

Figure 7: Left: H_2 conversion measured in ramp-up test mode as a function of temperature. Right: H_2 conversion measured in ramp-down test mode as a function of temperature.

The effect of the H_2:O_2 ratio on catalytic activity was examined using a Pt/HTO catalyst. The steady-state H_2 conversion at 75 °C was measured from stoichiometric (H_2:O_2=2) to fuel lean conditions (H_2:O_2=0.5). As shown in Figure 9, H_2 conversion increased under lean conditions; H_2 conversion was almost 100% at 75 °C with H_2:O_2=0.5 but only ~13% with H_2:O_2=2. The initial condition (H_2:O_2=2) was repeated at the end of the experiment and no change in the activity of the catalyst was seen during the course of the experiment. These results suggest that the H_2:O_2 ratio can be adjusted to regulate light-off temperature of the microhotplate. For example, during start-up, lowering the H_2:O_2 ratio would allow combustion to occur at a lower temperature, therefore less energy would be need to initiate the reaction. Once the flame was started, the H_2:O_2 ratio could be increased to increase the temperature, if necessary, for microFID operation.

Catalytic activation of the Pt/HTO supported catalyst was also found to occur following certain pretreatment conditions. After exposure to a rich environment (ramp-up and ramp-down to 600°C with H_2:O_2=3) the Pt/HTO catalyst was then tested under standard operating conditions (H_2:O_2=2) and was found to be extremely active at low temperatures (Figure 10). In fact, combustion occurred over the catalyst at room temperature. After this pre-treatment, the Pt/HTO showed similar activity to a commercial Pt/Al_2O_3 catalyst. Based on these results, room-temperature combustion would be possible with pretreatment under fuel rich conditions. This would limit the amount of microcombustor heating required to ignite the flame.

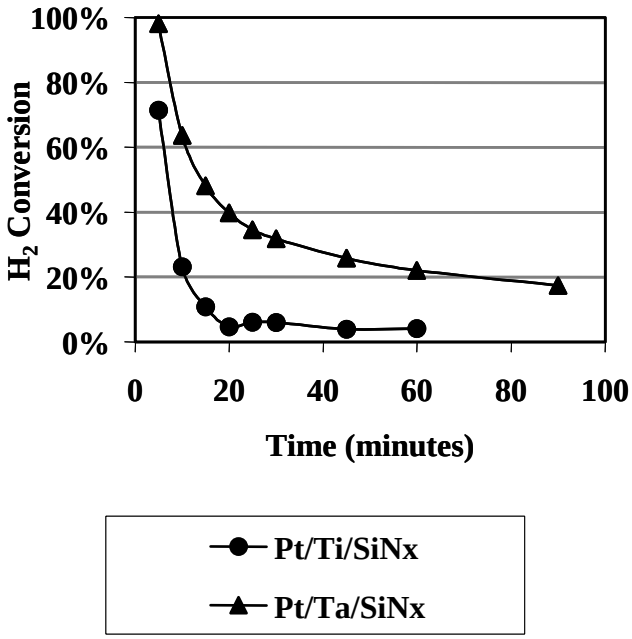

Figure 8: H_2 conversion measured as a function of time at 150°C.

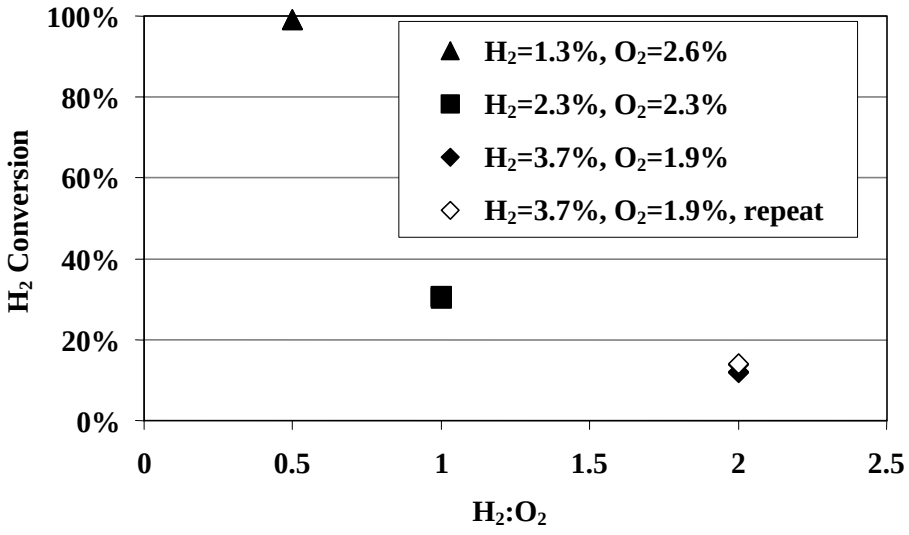

Figure 9: H_2 conversion as function of H_2:O_2 ratio at 75 ºC.

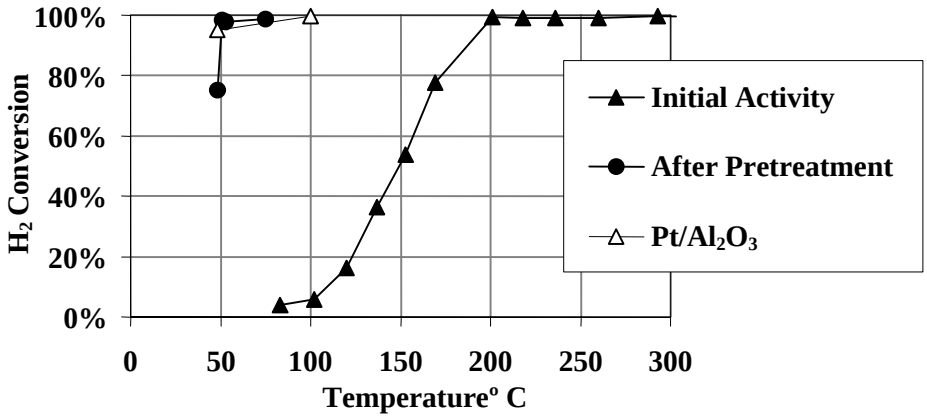

Figure 10: H_2 conversion as a function of temperature for Pt-HTO supported catalyst as prepared (initial activity) and after pretreatment under rich conditions at 600 ºC. Results from a commercial Pt/Al_2O_3 sample are shown for comparison.

Internally-developed, micropenned Pt/alumina

The u-tube performance of internally-developed Pt/alumina catalysts is roughly compared with Pt/HTO and Pd/HTO powders in this section. The behavior of the micropenned material is apropos to the section on microcombustor testing, since this type of material was used for that device. 1 wt% Pt in alumina was prepared in accordance with the description given in the Catalyst Deposition section and was micropenned onto test coupons of SiN on silicon; three samples, each with areas equivalent to that of a microcombustor, were printed. The Pt and Pd in HTO were also 1 wt% mixtures, but were left in the powder state. The powders were easily placed into the u-tube for testing and were packed with quartz wool. The micropenned samples, however, were placed into the tube and flow was reduced as much as possible to limit bypass of the samples by the combustible gases. The concentrations of CO, CH_4 and O_2 were monitored downstream from the samples. The data is presented in Figure 11.

CO was not present in the effluent so it was assumed that all the methane was converted to carbon dioxide and water. Also, methane conversion, based on methane concentration and oxygen concentration, agreed well. Comparison of the data on HTO powders and micropenned samples is complicated by the fact that the space velocities in both cases were so different. Again, for the micropenned materials, three uncrushed test samples were used and gas flows were lowered as much as the experimental apparatus would allow to help compensate for bypass effects. Light off for this sample occurred about 600 °C. It appears that due to bypass (gas flow not hitting the catalyst) the maximum conversion is about 60%. Considering the small amount of catalyst and bypass issue, this represents much more conversion than expected. For the Pt/HTO powder sample, light off on the ramp-up was significantly different than on the ramp down (data not shown); a suitable explanation for this behavior is not available at present. The Pd/HTO:Si sample had the lowest light off temperature, which is what is expected from the literature, and did not deactivate on the ramp down.

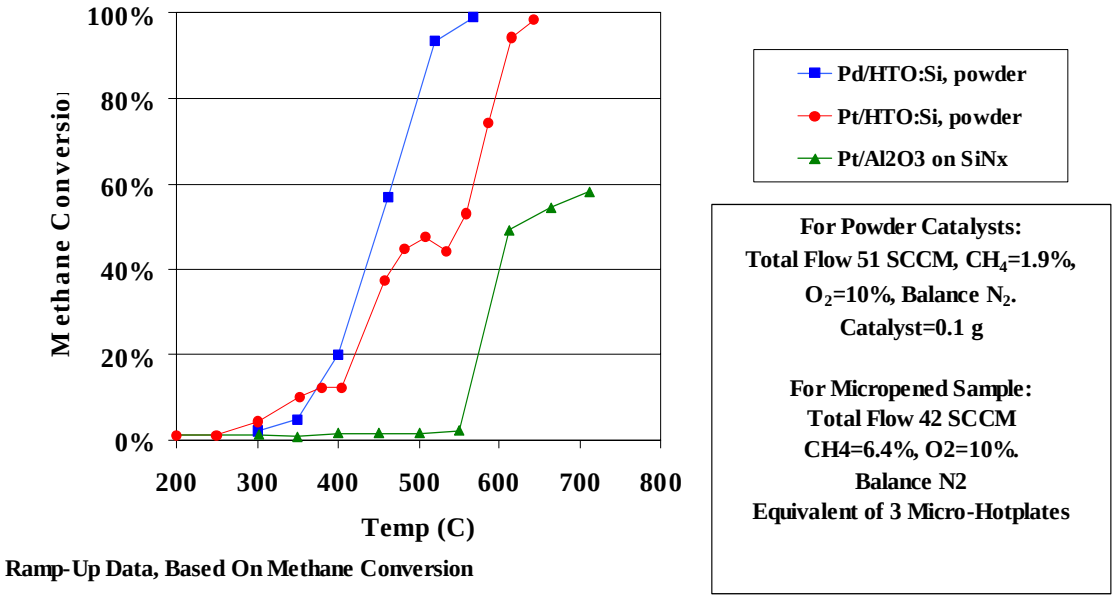

Figure 11: Methane conversion of various catalysts in both powder and micropenned forms.

Microcombustor and MicroFID Testing

Microcombustor testing in the drop-in test fixture

This section describes testing performed with the microcombustor in the drop-in test fixture with internally-developed, micropenned, alumina-supported catalysts. Testing regimes consisted of flowing various concentrations of hydrocarbons, air, and, in some cases hydrogen, into the fixture to combust over the microcombustor, which was set to a range of temperatures. The hydrocarbons were in concentrations of 0.8-40% of the total inlet gas composition, at inlet flow rates of 5-40 ml/min. The temperature of the microcombustor was set by an external circuit, and ranged from 83-600°C in these tests. Hydrocarbons tested include methane, ethane, propane and natural gas. In all tests dry air was used to dilute the hydrocarbon mixtures.

In addition to changes in inlet gas velocity, composition, and microhotplate temperature, a variety of different catalysts were tested on the microcombustors. The purpose of these different coatings was to perform speciation of the inlet gases using calorimetry and to understand the response of various catalysts for the purpose of heating. In addition to the catalysts, a coating of pure alumina was often placed on one of the two microcombustors in the test fixture. Since alumina is the base of both of the internally-developed catalysts, a coating of alumina acts thermally similar to them. This allows the creation of a reference source to help remove constant noise sources from the signal, such as fixture heating, circuit noise, or flow cooling.

During testing, the temperature of the microcombustor was controlled using a constant-resistance control circuit [17]. This circuit, which has moved from a preliminary breadboard design to a printed circuit board, varies the power into the microcombustor's heating element to maintain a set resistance. The set point resistance, and therefore temperature, is user controlled. The circuit can drive and monitor two microcombustors at once. When external heating from combustion attempts to increase the effective resistance of the heating element, the circuit power decreases to compensate. This feedback mechanism maintains constant microhotplate resistance, and hence constant temperature. The magnitude of these fluctuations about the baseline power constitute the measured signal of the sensor and allow direct measurement of the combustive heat collected by the device. The advantages of constant temperature operation include reduced signal variability from temperature fluctuations, longer microhotplate life from a reduction in thermal cycling, and assurance that microcombustor temperature does not change with ambient gas concentration [3].

Figure 12 shows a graph of the signal from a microcombustor, held at 500 °C, during combustion of natural gas [18] in concentrations of 1.78%, 3.51%, 5.17%, and 6.78%. The figure shows that for 1.78% of natural gas, a signal of 7 mW is returned within one minute of combustion. Hydrocarbon injections into the fixture produced an almost immediate signal response. However a settling time of approximately 1 second was evident in all cases. While the response time of the circuit and device was very fast, the hydrocarbon must uniformly fill the internal volume of the fixture before it can produce a steady signal.

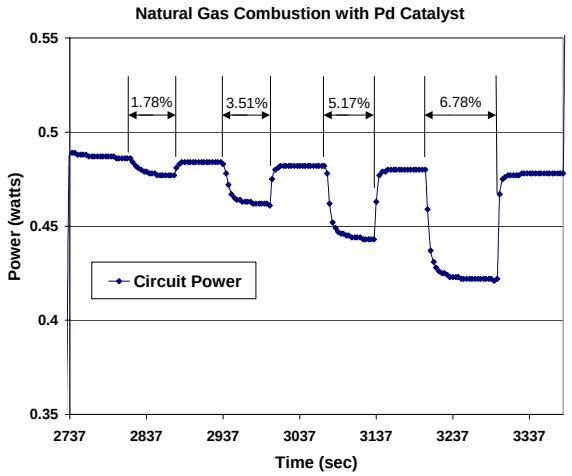

Figure 12: Microcombustor signal from natural gas combustion with a Pd catalyst.

MicroFID testing with the glass lid electrode

The approach taken in this work to miniaturizing an FID was fundamentally different from previously reported work. Previous work uses a conventional FID as a blueprint for miniaturization [8]. As with conventional FIDs, multiple gas inlets were used: one for hydrogen, and another for oxygen and the analyte gas. These two gas streams were then brought together to react and combust. By way of contrast, in the work reported here, premixing and a single gas inlet that injects hydrogen, air, and analyte gases simultaneously was used; in the future, separate flows could be used if desired. The ignition source in this device comes not from heating of the gases or a spark igniter, but from the Pt catalyst that is heated by the microcombustor. The catalyst has the advantage of not only allowing low-temperature combustion of the gases, but it also promotes stabilization of the flame.

Two separate circuits were used in the FID experiment, the constant-resistance circuit described above for regulating the microcombustor temperature, and an electrometer circuit for measuring the current generated by catalytically-stabilized oxyhydrogen combustion of analytes. Constant-temperature operation of the microcombustor was found to be important, as described below. The electrometer circuit measures ionization current generated in the flame plasma and accelerated between the lid and microcombustor electrode by an externally-applied voltage (Figure 13). The electrometer, designed and built in house, uses a Burr-Brown OPA129 op-amp and 8^{th}-order Bessel filtering to amplify the ionization current and to filter unwanted noise, including 60 Hz line noise (Figure 14). Using a Keithley 220 current source, a gain of 12.5 mV/pA was demonstrated with presently used circuit gain factors; e.g., a 100 pA input, yields 1.25 V output (Figure 15).

During experimentation, the total gas flow was restricted to 60 ml/min. Of this amount, about 11% was composed of hydrogen, a range of 1.16%, 1.74%, 2.3%, and 2.86% was composed of ethane, and the balance was dry air. Ethane was chosen as the initial test gas due to the relative ease in cracking as compared with methane. The potential between the lid electrode and the electrode on the surface of the microhotplate was 20 volts. The literature reports that a much higher potential is usually necessary, however good results were obtained here with this lower value. The constant-resistance control circuit was engaged, and the gases were fed into the small combustion chamber. When combustion initiated inside the chamber, even without the presence

of analyte gas, a 1 volt offset on the FID signal was obtained. This offset is of an unknown source, however it may indicate gas-phase connectivity between the two circuits or surface ionization. The signal size during the combustion ranged between 170 mV and 1.19 V, which indicates that the electrometer circuit was performing the necessary signal gain. When the constant-resistance control circuit was turned off, the voltage offset immediately returned to zero, however the signal of the FID inverted. This further bolsters the interpretation of electrical cross-talk between the circuits during their operation and indicates that an improved grounding scheme and/or electrical isolation covering the heater metal should eliminate this effect.

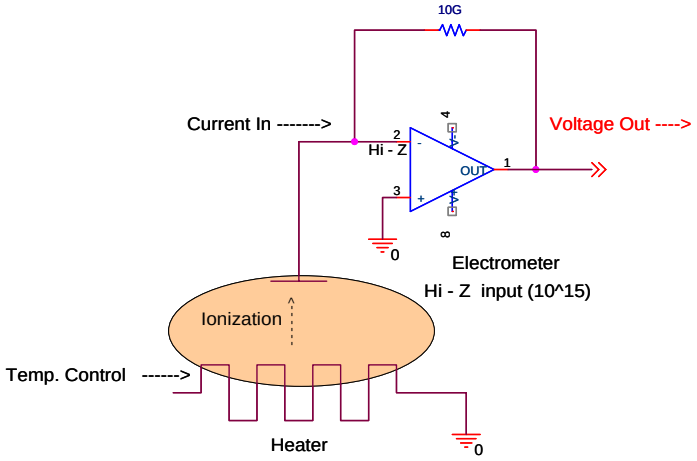

Figure 13: MicroFID schematic showing operation of the electrometer circuit.

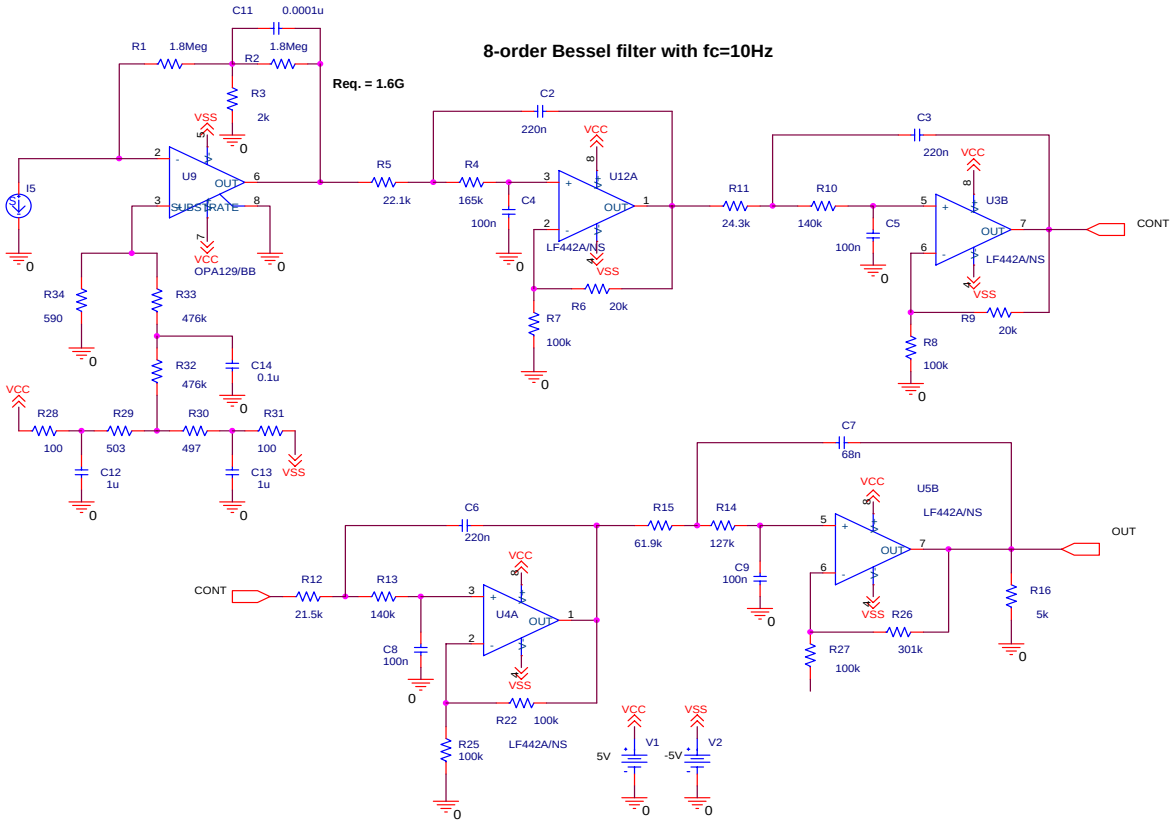

Figure 14: Electrometer circuit diagram.

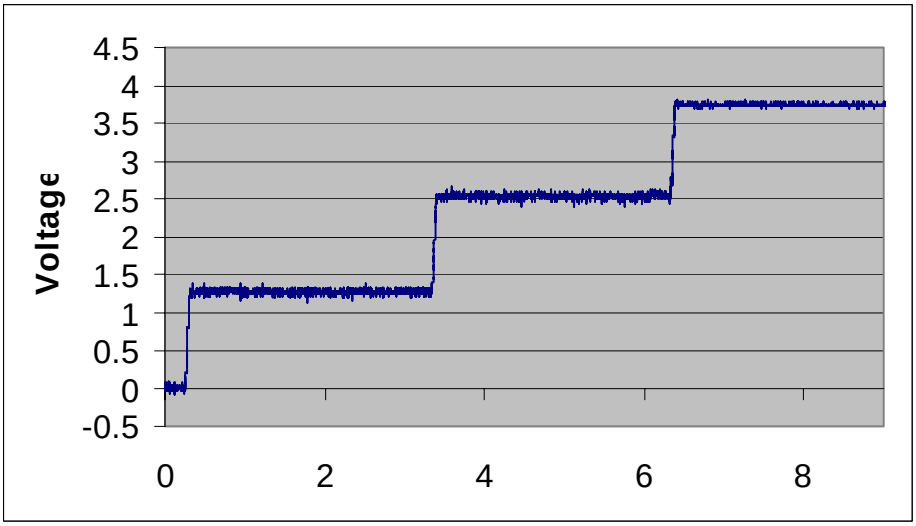

Figure 15: Signal response of electrometer circuit to 100 picoamp input steps.

Data analysis

Microcombustor data

Testing has shown that the operating regime of the microcombustor array was quite large, and ranged from the low-temperature oxidation of hydrocarbons, to full combustion with hydrogen. All of the hydrocarbons tested were successfully combusted. These tests have also shown that catalytic combustion increases the hydrocarbon limits of flammability (LoF). Table 1 summarizes these expanded limits of flammability. The final limits of these hydrocarbons have not been reached in these tests; so continuing increases in the upper and lower ranges are expected. The results shown were valid for both Pd and Pt catalysts.

Table 1: Comparison of conventional and unoptimized catalytic combustion

Hydrocarbon	Conventional Limits of Flammability	Catalytically-Stabilized Limits of Flammability
Natural Gas	4-16%	1.3-35.5%
Methane	5-15%	2-20%
Ethane	2.9-13%	1-4%*
Propane	2.1-9.5%	1-11.5%

*Ethane has not yet been tested beyond the upper limit of flammability.

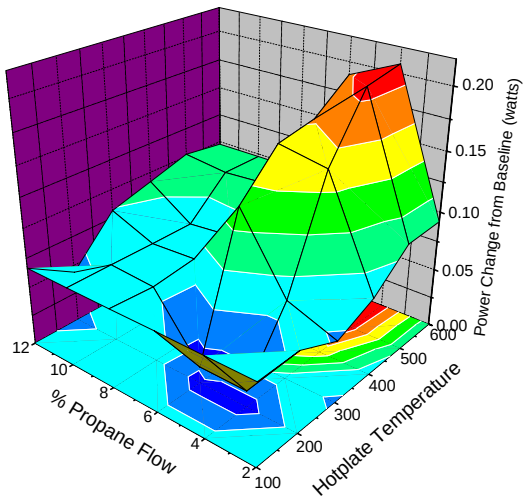

Figure 16: Response surface of propane to temperature and flow concentration.

The signal results demonstrated that all hydrocarbons generated detectable amounts of heat down to a thousand ppm or less. Each hydrocarbon exhibited combustion behavior dependent on the flow rate of the inlet gas, microcombustor temperature, and the concentration of the hydrocarbon in the gas stream. In general, there appears to be a strong correlation between the stoichiometric ratio of hydrocarbon to oxygen, and the peak hydrocarbon concentration for combustion. The stoichiometric ratio for propane is 4%, and the concentration of peak combustion for propane in these tests appeared to be around 5%. For methane, this ratio is about 10%, and testing described here indicated an 11% concentration was optimal. This correlation was valid for only high flow rates, however. In the low flow regime, there are cases for which stoichiometric mixtures

actually have lower signals than non-stoichiometric mixtures. There was also a heavy signal dependence on the inlet flow rate; higher flow rates tended to produce larger signals. As the flow rate was increased, stoichiometric mixtures begin to dominate. The exact mechanism for this is unknown, however it may be that at higher flow rates combustion products were swept downstream from the microcombustor more quickly, allowing the catalytic reaction to take place closer to its maximum efficiency. Microcombustor temperature largely increased the signal response, however at higher concentrations of hydrocarbon, the signal may actually decrease with increasing temperature. This signal inflection point was dependent only on catalyst, not inlet gas velocity or composition. Enough data has been taken across various microcombustor temperatures, flow rates, and hydrocarbon concentrations to create response surfaces, and Figure 16 shows a typical response surface for propane.

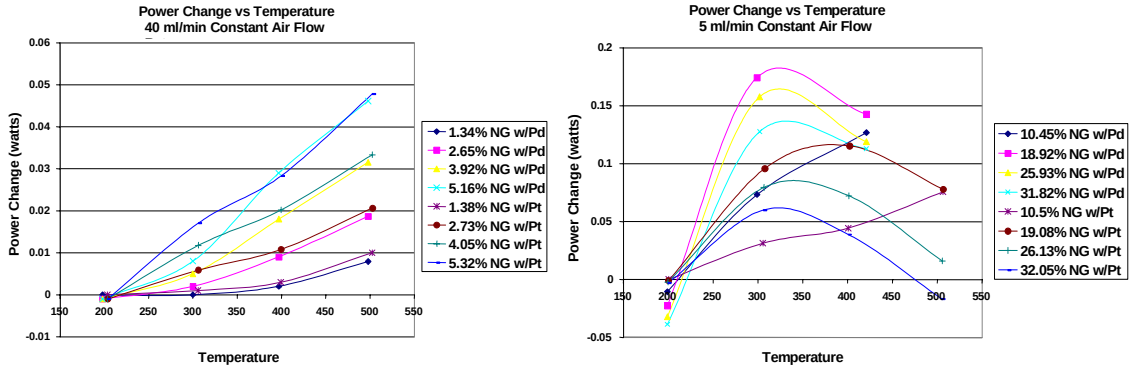

Figure 17: Power change comparisons of Pt and Pd catalysts at 40 ml/min and 5 ml/min.

Extensive data analysis was done to determine the differences between the combustion profiles of the Pt and Pd catalysts. According to the literature [19], a Pd catalyst is sensitive to all hydrocarbons above 400 °C, while Pt is sensitive to all hydrocarbons, except methane, at temperatures below this. During natural gas combustion tests it was found that the Pt and Pd catalysts exhibited slightly different combustion characteristics. These differences should aid in the determination of the methane content of incoming gases. In general, the platinum catalyst combusted hydrocarbons more effectively over all tested airflow regimes, except for the lowest of 5 ml/min. The specific point where the Pd catalyst becomes more effective is unknown, but was between 5-10 ml/min of flow. Figure 17 shows comparisons of the two catalysts for the 40 and 5 ml/min airflow, respectively. It was also determined that the temperature of the signal inflection point mentioned above was dependent on catalyst: 400 °C for Pt, and 450 °C for Pd. At present, the reason for these behaviors have not been determined, though continuing work will explore this.

To further characterize the differences in combustion, response surfaces were created for the two catalysts. Figure 18 shows the response surfaces of natural gas combustion differentiated by Pd and Pt catalysts. Tools such as these can be used to determine the optimum combustion points in terms of concentration, especially when used in conjunction with catalyst combustion profiles. In the case of a microcombustor array utilizing multiple catalysts, testing at the highest and lowest flow regimes, with Pt and Pd catalysts respectively, would likely yield the maximum signal differential for speciation.

Another use of the microcombustor is the determination of the total heating value of the inlet gas. Despite the fact that the volume of the drop-in test fixture used in these experiments was too large

to allow for complete combustion of all the fuel, gas combustion occurred in reasonably repeatable amounts. Table 2 shows that the microcombustor routinely combusted repeatable amounts of hydrocarbon, no matter the hydrocarbon concentration, with average efficiencies deviating by a maximum of 5%. This likely indicates that the catalytic combustion occurs in the vicinity of the catalyst coating. To bolster this view, further analysis shows that the majority of injected hydrocarbons are not combusted: combustion of 15.78% methane in a gas flow of 10 ml/min with a microcombustor at 600 °C produced 158 mW. A mole of methane at room temperature and atmospheric pressure will occupy 24,290 ml and will produce 802 kJ when perfectly combusted. In the data mentioned above, this would amount to 1.578 ml/min of methane flowing into the fixture. Assuming perfect combustion, approximately 860 mW will be liberated. Given the signal change, of 158 mW, this corresponds to only 18.37% of the total combustion energy possible being detected. Since the microcombustor was a capable temperature sensor, with a sensitivity of ~1mW/°C, this showed the majority of the hydrocarbons bypass the microcombustor due to the relatively large internal fixture volume. In the future, different natural gas formulations will be combusted, and compared to these results. If the efficiencies are truly repeatable, then the relative heating values of various fuels will be truly discernable. Furthermore, packaging with smaller internal volume is envisioned in the future, reducing bypass effects.

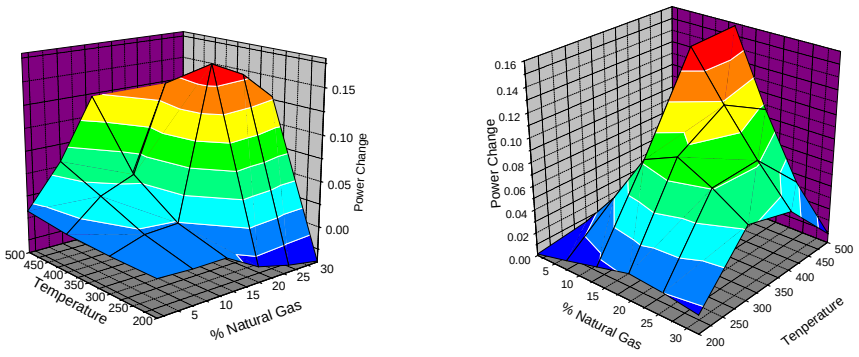

Figure 18: Natural gas response surfaces of catalytic combustion with Pd and Pt respectively.

Table 2: Signal analysis to determine combustion efficiencies.

Hydrocarbon	Catalyst	Inlet Air Flow	Hydrocarbon Concentration	Average Combustion Efficiency
Natural Gas	Pt	10 ml/min	6.92%	15.3%
Natural Gas	Pd	10 ml/min	17.92%	10.23%
Methane	Pt	10 ml/min	20%	9.27%
		30 ml/min	7.69%	11.45%
Propane	Pt	10 ml/min	11.5%	9.18%
		30 ml/min	4.15%	12.7%

Preliminary studies have also been performed using hydrogen to aid in combustion. These results will not be presented here in detail, as the work is still preliminary, however initial indications show that the combustion of hydrogen concurrently with hydrocarbons results in greater

sensitivity of the device to hydrocarbons. Likely this result can be explained by an abundance of H+ radicals chemically cracking the hydrocarbons, the effect of which would be complimentary to the Pt or Pd catalyst reaction.

Microcombustor for microsystem heating

Our testing indicates that catalytic combustion was easily achievable, and sustainable, with current devices and catalyst formulations. With sustainable combustion comes the option of using the micro hotplate device for the heating of GC columns or other microsystems. When compared to conventional batteries, a hydrocarbon combustion scheme allows for a large increase in stored energy. Energy density for conventional dry chemistry batteries is extremely low when compared to propane and other hydrocarbon mixtures, with a typical high performance lithium ion battery having an energy density of 79.2 J/g, while the equivalent mass of propane would release 46.33 kJ of energy. Our testing indicates this hydrocarbon combustion approach may be viable. Empirically, it was noticed that the aluminum test fixture warms during the process of testing. Thermocouple data from within the fixture indicates air temperatures inside the fixture of 50-60°C are routinely reached over the course of a single run, which indicates a large release of energy has occurred inside the fixture.

Unfortunately, since the fixture is not optimized for the combustion of hydrocarbons or the resulting containment of the released heat, we must extrapolate heating efficiency from our present results. Signal analysis shows that the majority of injected hydrocarbons are not combusted, as they likely blow by the catalyst and flame due to the large internal fixture volume. Analysis was performed on a data set that shows the combustion of 15.78% methane in a gas flow of 10 ml/min with a micro hotplate at 600 °C. A mole of methane at room temperature and atmospheric pressure will occupy 24,290 sccm and will produce 802 kJ when perfectly combusted. In the data set mentioned above, this would amount to 1.578 ml of methane flowing into the fixture per minute. Assuming perfect combustion, approximately .86 W will be liberated. Given our signal change, of .158 Watts, this corresponds to only 18.37% of the total energy possible from combustion being detected. Since the micro hotplate is an extremely capable temperature sensor, with a sensitivity of .001 W/°C, this shows the majority of the hydrocarbons are blown by the microcombustor. This analysis did not take into account the energy lost through warming of the fixture or the surrounding gas stream, or inefficiencies in detection or combustion, however it serves as an approximation of energy release. We can perform a similar analysis for propane. Figure 19 shows the signal power change caused by propane injections into the gas flow. In the 4.15% propane concentration case, the overall efficiency of combustion is only 12.68%, however it still releases .221 W, which corresponds to about 35.36 $mW \cdot (mm^2)^{-1}$. If a compressed vial of propane gas supplemented the battery power of the micro chemlab, then the energy lifetime of the system could be greatly extended in the field. Even with this inefficient combustion, across a 13 x 13 mm square silicon die, which is the approximate size of the micro GC, we would see 5.975 watts of power being applied to the device which would heat it to 120°C in about 8.7 seconds. For comparison, the conventional electric heaters on the micro GC require 20 volts to supply the 6.8 watts necessary to raise the steady state temperature of the GC to 120°C in 7 seconds. These energy requirements for electrical heating of the micro GC are already a factor of 10 lower than conventional systems. A small battery would be needed to provide the initial heating of the catalyst, but after this has occurred the catalytic combustion should release enough energy to keep the system at a high steady state temperature. Propane would be a good choice for the hydrocarbon because of its high energy density, availability, and its familiarity to users of the prospective microchemlab system.

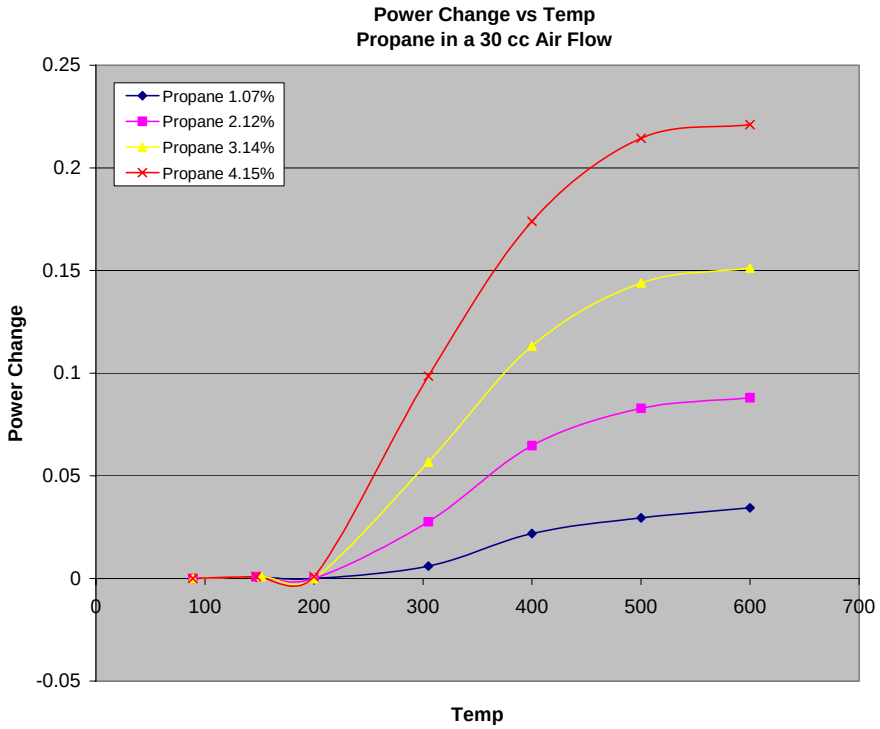

Figure 19: Power change from baseline caused by propane injection

MicroFID data

Analysis of the microFID data shows good signal fidelity and response time to ethane combustion. Figure 20a shows the response of the FID to 1.2-2.9% ethane. The FID signal increased immediately after analyte injection, though there was an observed settling time; 1.2% ethane yielded a signal of 0.17 volts, indicating a reasonable preliminary sensitivity for this sensor. This was especially noteworthy considering the low, 20 V, potential applied to the collection electrodes, the small surface area of the driving electrode, which is less than 0.17 mm^2, and the non-uniformity of the potential field caused by the meandering electrode pattern.

Figure 20b shows the FID signal after the constant resistance control circuit has been turned off. The same range of ethane concentrations, at the same flow rate, was used. Aside from the obvious cosmetic changes to the signal, from the issues described in the testing section above, the signal sensitivity decreases, likely due to variability in the combustion temperature. With the control circuit turned off, the microcombustor was no longer at a set temperature, and the catalyst material likely had large thermal gradients across its surface. Comparison of the two figures below shows significant differences between the two modes of sensing. The temperature control promotes higher sensitivity, by about a factor of 3 for the lowest ethane concentrations. For the higher ethane concentrations the signal was of the same magnitude. The constant temperature control also increased the speed of the steady-state signal response. These results confirmed that maintenance of flame temperature was an important operational practice with beneficial results.

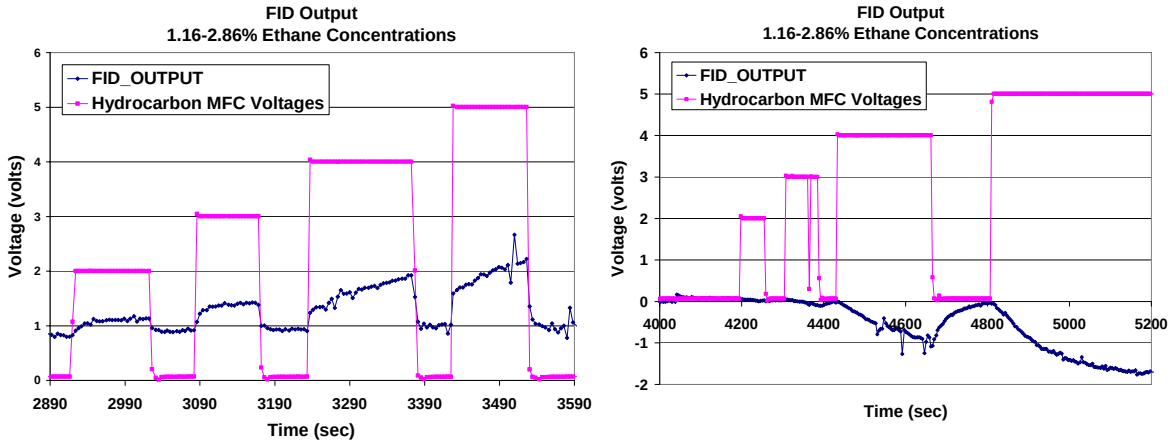

Figure 20: FID output with and without the constant-resistance control circuit.

Modeling

Three separate modeling/simulation efforts were undertaken in this project to understand various aspects of the behavior of the microcombustor. The first such effort involved fundamental modeling/simulation of the ignition/extinction behavior of the microcombustor. Simulations in Chemkin and Aurora were also performed to predict operation temperatures and to verify the importance of the catalyst surface in microcombustor performance. Finally, finite-element thermal modeling of the use of the microcombustor in heating a microanalytical system was performed.

Fundamental analysis in stagnation point flow

Based on the conditions realized in the original microcombustor experiments utilizing glass lids on DIP packaged microcombustors, an idealized geometry corresponding to a premixed flame in stagnation-point flow was used to investigate the ability of catalysis to extend the extinction limits of nonadiabatic, stretched flames (Figure 21a) and to thus compensate for increased thermal losses associated with larger surface-to-volume ratios. Specifically, a surface catalytic reaction was assumed to occur on the stagnation plane, thereby augmenting combustion in the bulk gas with an exothermic surface reaction with a lower activation energy. Based on the fact that the activation energies remain large, an asymptotic analysis of the resulting flame structure yields a formula for the extinction limit as a function of various parameters. Figure 21 (bottom) shows typical results of this analysis in terms of the perturbation in surface temperature (θ_s) plotted as a function of the nondimensional strain rate (α_1), which reflects the rate of flame stretching. With respect to Figure 21 (bottom), the largest value of α_1 beyond which no solution exists (denoted by a solid circle at the maximum value of α_1) defines the extinction limit, where the additional solid circle on each curve marks the corresponding extinction limit in the absence of catalysis. For parameter values that reflect the present experiment, the catalytic surface reaction extends the extinction limit to a larger value of α_1 and can thus compensate for increased values of a loss parameter Ψ. The latter reflects a linear combination of conductive thermal losses at the catalytic surface, volumetric heat losses associated with the finite size of the combustor, and convective losses associated with ratios of thermal to mass diffusivity greater than unity. This extension of the extinction limit due to the presence of a surface catalyst extends the combustion regime, thus counterbalancing the effects of heat loss and flame stretch that tend to shrink it.

The surface-temperature response illustrated in Figure 21b also indicates the possibility of multiple solution branches, or operating states. A separate stability analysis of these steady, planar solutions shows that all branches are linearly stable, suggesting that multiple stable operating states can coexist. Consequently, the observed flame behavior is likely to depend on external influences such as initial conditions, making it possible to observe different operating states for a given experimental configuration. The present results corresponding to the particular μCombustor of interest here are relevant to small-volume combustors in general, where the increased surface-to-volume ratio can lead to extinction of the nonadiabatic flame in the absence of a catalyst.

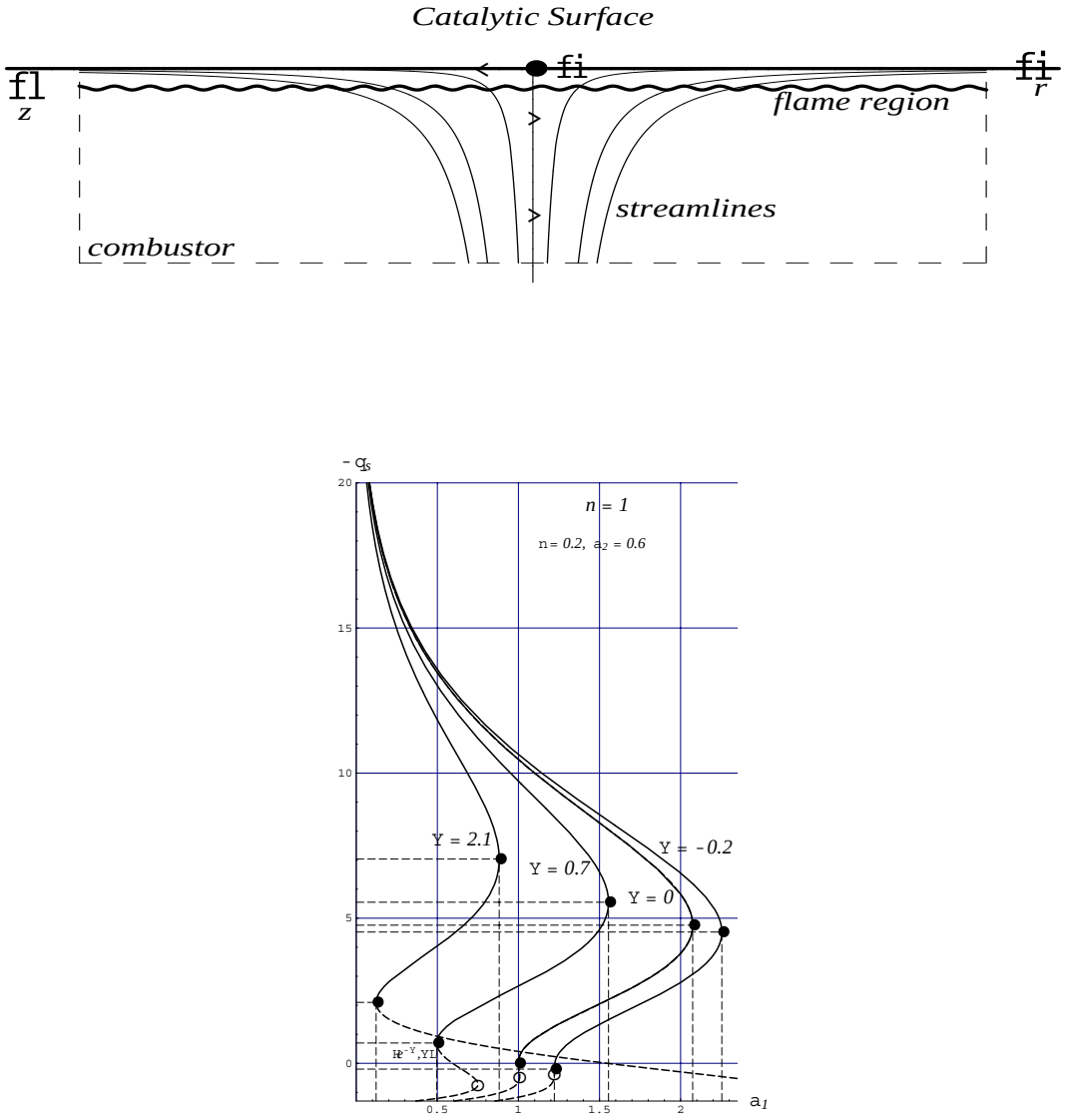

Figure 21. Idealized catalyst-assisted stagnation-point flame near extinction (top), and the corresponding response of the surface-temperature perturbation θ_s as a function of the nondimensional strain rate α_1 for various values of the loss parameter Ψ (bottom). The largest value of α_1 beyond which no solution exists (denoted by a solid circle at the maximum value of α_1) defines the extinction limit, where the additional solid circle at $-\theta_s = \Psi$ on each curve marks the corresponding extinction limit in the absence of catalysis. For parameter values that reflect the present experiment, the catalytic surface reaction extends the extinction limit to a larger value of α_1 and can thus compensate for increased heat losses (larger values of Ψ).

Chemkin and Aurora modeling

Chemkin was used to model supported oxyhydrogen combustion in small geometries. The exact flow patterns cannot be modeled in Chemkin, so idealized simulations were run using Aurora, a continuous stirred tank reactor (CSRT) model. Total reactor volume was modeled based on the original prototype glass-lid microcombustor. In order to discriminate between the rector walls and the catalytic surface, a fraction of the surface was entered to be platinum. The H_2:O_2 reaction mechanism on the platinum surface and homogeneous reactions were taken from C_2H_6-O_2-H_2 reaction that had been modified to reflect results developed at Los Alamos National Lab (1999) and includes the Zerkle/Tummala-Williams data fit.

Aurora uses a continuously-stirred tank reactor, and all temperatures were assumed to be homogenous throughout; therefore, it was impossible to determine variation in the flame temperature and the differences between the temperature on the microhotplate surface and in the flame region. For all the test simulations, either 0% or 100% steady-state H_2 conversion was obtained, unlike in actual microcombustor testing where intermediate conversions are of course possible. Assuming a total flow rate of 0.3 sccm, 15% H_2, 25% O_2 and 60% N_2, the steady state temperature was found to be 755 ºC. This is a homogenous temperature, however, in actual device testing localized hot spots could occur. Based on this result, it is not surprising that at these temperatures microhotplate failures sometimes occurred. Due to the limitations in using this model for a complex geometry and flow pattern, the quantitative numbers produced are not likely to reflect of actual values in the microcombustor. However, it is reasonable that the trends and qualitative results are applicable in microcombustor application and design.

The Pt catalyst was shown to be necessary for reasonable ignition of the oxyhydrogen flame. Under stoichiometric conditions very high initial temperatures were necessary to ignite the flame without platinum. Under very lean conditions H_2:O_2=0.4, no steady-state combustion was predicted without a platinum catalyst, regardless of the initial temperature, even when assuming adiabatic conditions. These results suggest that, as anticipated, the presence of the platinum catalysts extends the range of possible operation for combustion. This is in agreement with fact that no flames were observed during microcombustor operation with the Pt catalyst film covered.

Not surprisingly, increasing the total amount of H_2 available to the flame either by increasing the total flow rate of all gases or by increasing the H_2:O_2 ratio was found to increase the temperature inside the reactor. Similar to the results from the u-tube reactor, the initial temperature necessary for combustion increased with increasing H_2:O_2 ratio. Increasing the heat transfer coefficient would decrease the temperature in the CSRT. If the heat transfer coefficient was too large, then the flame could not reach steady state combustion even with the catalytic platinum surface. This highlights the need for insulating, to some extent, the microcombustor. These results are in general agreement with the catalytic experiments and results from actual microcombustor experiments, and may serve as a starting point for future modeling with a 3-D resolution of the flame.

ANSYS finite element thermal modeling

To validate the use of the microcombustor in microsystem heating, an important test case was considered: heating of a micro gas chromatography column (microGC). This example is pertinent because it represents the upper limit of heat energy required in microsystems, since the microGC is typically much larger than other microanalytical systems. Also, microGCs are very important microanalytical components, often in need of heating to enhance their performance. A

simple 3D model of a micro GC was created in the ANSYS finite element modeling software package. The model consisted of a GC sized silicon die, a glass lid bonded to the die, and the Pyrex gas inlets which elevate the system above the circuit board. This setup was identical to that used in the Microchemlab system [20]. A uniform heat load of 35.36 mW/mm^2 was added to the back of the microGC die, which is the energy associated with catalytic combustion of propane, and appropriate boundary conditions were included from thermistor readings taken during experimental microGC heating. The purpose of this model was to ascertain whether the energy released during catalytic combustion was enough to uniformly heat the microGC to the desired temperature of 120°C. Figure 22 shows a cross-sectional view of the ANSYS modeling results. The microGC column die is on the top of the stack, with the Pyrex lid shown on the bottom. From these results we can see that the microGC is uniformly heated to the necessary temperature.

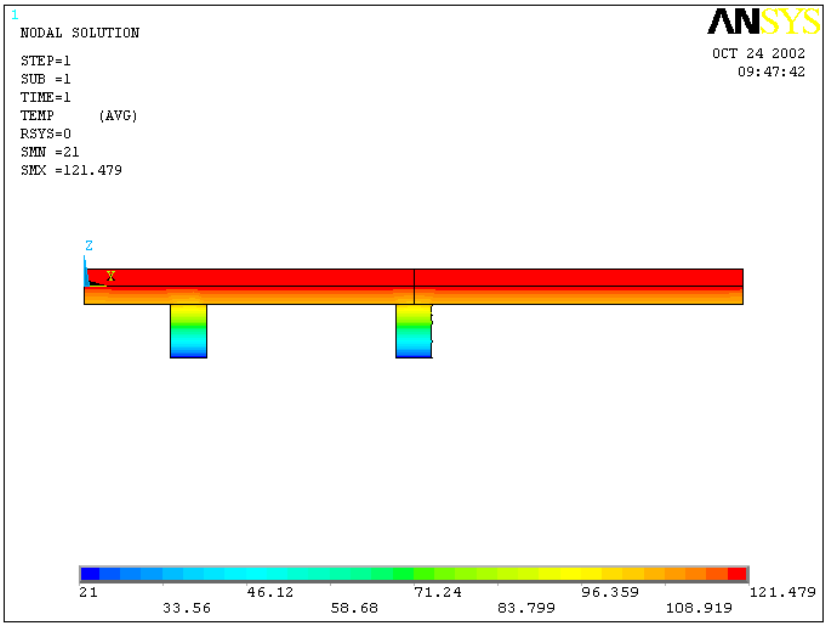

Figure 22: Thermal model of a Micro-GC stack heated by hydrocarbon combustion.

Modeling/simulation of the microcombustor was undertaken to understand ignition/extinction behavior and failure modes. Fundamental studies of ignition/extinction explained catalytic extension of LoF despite enhanced microdomain heat losses; these studies also showed the possibility of multiple operating points. Simulation in Aurora, a continuously-stirred reaction model, predicted average temperature increases and helped explain premature failure of the microcombustor under certain operating conditions. It also confirmed the importance of the catalyst surface in microcombustor operation. Finally, thermal modeling showed the feasibility of heating microsystems, such as the microGC column, using the microcombustor.

Summary

FY02 was a successful year for this project. Critical advances in supported catalysts, as well as improvements in fixturing, and data acquisition/analysis, allowed almost all of the annual and overall project goals to be satisfied. In previous years, thin-film platinum or drop-coated commercially-available catalysts were used to initiate/sustain combustion on the microcombustor. At combustion temperatures, the thin-film catalyst routinely failed due to delamination, hotspots and metal agglomeration, induced by metal migration. The commercially-available catalysts were difficult to obtain and methods for controlling its deposition were lacking. Two steps were taken to address these problems. First, alumina-supported automotive catalysts were prepared in house. Thus far, 1wt% Pt or Pd have been tested. These materials were then prepared for micropenning. Humectants minimized cracking of the thin catalysts. Importantly, these techniques have permitted precise depositions of catalysts on the microcombustor; control of the catalyst boundaries is ~25-50 microns and catalyst thickness have been applied down to 15 microns total thickness.

The PEEK fixture described in previous reports was abandoned due to volume restrictions and temperature incompatibility. Another fixture, with slightly larger volume and made from aluminum, was designed and built; the fixture allowed for visual inspection, thermocouple inputs and the ability to control the inlet height, internal volume, and had exit ports adequate for water vapor egress.

The new fixture, improved catalysts, and new automated data acquisition/analysis systems permitted an experimental combustion matrix. The microcombustor was heated to initiate/sustain combustion, using an in-house constant-temperature circuit, implemented this year on a circuitboard. The combustion of hydrogen, methane, ethane, propane and natural gas (NG), in air, were evaluated with flow rates from 5 – 40 ml/min and concentrations from 2.5-40%. For all gases studied, the limits of flammability (LoF) were extended via micropenned catalysts relative to conventional flames. For example, an unoptimized NG LoF of 1-32% was obtained, whereas conventionally 4-16% is observed. Although originally butane use was intended for microcombustor heating, only the abovementioned fuels were used. Nonetheless, unoptimized heating of 38 mW/mm2 was observed for NG, a fuel source as common as butane, though not as energy intensive. This work shows the viability of using common fuels in microcombustor heating of Microsystems.

A conventional u-tube reactor was used to independently verify catalyst performance and understand catalyst activation/deactivation. This year, tests were performed on micropenned Pt/alumina, and bulk catalysts, to study light off and methane conversion. During these tests, the micropenned samples demonstrated behavior similar to bulk catalysts.

Modeling/simulation of the microcombustor was undertaken to understand ignition/extinction behavior and failure modes. Fundamental studies of ignition/extinction explained catalytic extension of LoF despite enhanced microdomain heat losses; these studies also showed the possibility of multiple operating points. Simulation in Aurora, a continuously-stirred reaction model, predicted average temperature increases and helped explain premature failure of the microcombustor under certain operating conditions. It also confirmed the importance of the catalyst surface in microcombustor operation. Finally, thermal modeling showed the feasibility of heating microsystems, such as a microGC column, using the microcombustor.

Finally, flame-ionization detection on the microscale was demonstrated this year. Original DIP packaging was used to take advantage of previously machined flow lids with integrated electrodes. Commercially-available catalysts were used since this demonstration took place prior to micropenning. Essential to this demonstration was the development of an electrometer capable of detecting the picoamp signal expected. This circuit was modeled, breadboarded and tested. Accordingly, a circuitboard version was implemented. 100 pA gave 2 V output; 10 pA steps were discernable, and a noise floor of about 1-2 pA was observed. To demonstrate the FID, 20V was established between the electrode in the lid and a counter electrode on the microcombustor. An oxyhydrogen flame was established and propane was introduced; the gases reaching the microcombustor were premixed, atypical for FID, but easy to achieve with our existing apparatus. Nonetheless, flame ionization did occur and concentrations of 1-4% of propane were easily detected. This is the first ever demonstration of flame ionization detection on the microscale using catalytically-stabilized combustion using premixed fuel/air/analyte.

Conclusions and Future Directions

By using a microhotplate for catalyst heating, a microcombustor has been developed that permits sustainable combustion on the microscale despite enhanced heat losses in this domain. Not only does the microcombustor permit stable flames in the microdomain, but also expands the limits of flammability (LoF) as compared with diffusion flames. This has important consequences for its use in microanalytical systems, including reduced fuel supply size and device lifetime.

Two main applications of the microcombustor were investigated in this work, microsystem heating and micro flame ionization detection. Calorimetric gas sensing was also studied in a parallel effort [21] and those results are summarized. Heating of microsystems using the microcombustor was shown to be feasible even for large microsystem components like microGC columns. This work reports the first-ever demonstration of flame ionization detection on the microscale using lean, premixed fuels and catalytically-supported flames. Speciation of hydrocarbon fuels also seems possible with this technology.

Overall, this work represents is a critical step in the direction of heated microsystems and combustion-based detectors for microsystems. But further work is of course needed to make these devices more widely available. Future work should include the following: (1) Determination of the optimum catalysts for heat generation and fuel speciation. (2) Expansion of the operation ranges of the microFID in terms of gases, gas concentrations, microhotplate temperature and flow rate. (3) Improvements in microcombustor robustness, likely through the use of higher-temperature metals and adhesion layers, and the metal passivation using dielectric overcoats. (4) Development of new catalysts for higher-temperature operation and/or improved conversion. (5) Further miniaturization to include microfluidics, and the inclusion of integrated electrodes and front-end detection electronics for the FID.

Patents and Publications

This section describes patents, publications and presentations resulting from this project.

Patents

Microcombustion Device for On-Chip Thermal Energy, SD-6850, Provisional Patent, filed 2/19/02.

Publications

M.W. Moorman, R. P. Manginell, C. Colburn, D.L. Mowery-Evans, P.G. Clem, N.S. Bell, L.F. Anderson, Microcombustor array and micro-flame ionization detector for hydrocarbon detection, SPIE Micromachining and Microfabrication Conference Proceedings, Santa Clara, CA, 1/25-31/2003, to appear.

S. B. Margolis and T. J. Gardner, Extinction Limits of Nonadiabatic, Catalyst-Assisted Flames in Stagnation-Point Flow, *Combustion Theory and Modelling*, 6 (2002) 19-34.

S. B. Margolis and T. J. Gardner, "An Asymptotic Model of Nonadiabatic, Catalytic Flames in Stagnation-Point Flow," *SIAM Journal on Applied Mathematics* (2002) to appear.

SAND2001-8172

SAND2002-8025

Presentations

M.W. Moorman, R. P. Manginell, C. Colburn, D.L. Mowery-Evans, P.G. Clem, N.S. Bell, L.F. Anderson, Microcombustor array and micro-flame ionization detector for hydrocarbon detection, SPIE Micromachining and Microfabrication Conference, Santa Clara, CA, 1/25-31/2003, to be presented.

D.L. Mowery, R.P. Manginell, T.J. Gardner, G.C. Frye-Mason, R.J. Kottenstette, Development of a novel on-chip combustor device, North American Catalysis Society Meeting, Toronto, Canada, 6/3-6/8/01.

D.L. Mowery, R.P. Manginell, T.J. Gardner, G.C. Frye-Mason, R.J. Kottenstette, Development of a novel on-chip combustor device, Western States Catalysis Conference, Provo, UT, 2/23/01.

S. B. Margolis and T. J. Gardner, Extinction Limits of Nonadiabatic Catalyst-Assisted Flames in Stagnation-Point Flow, Second Joint Meeting of the US Sections of the Combustion Institute, Oakland, CA, 2001.

S. B. Margolis and T. J. Gardner, Extinction Limits of Nonadiabatic Catalyst-Assisted Flames in Stagnation-Point Flow, 2001 International Mechanical Engineering Congress and Exposition, New York, NY, 2001.

S. B. Margolis and T. J. Gardner, Extinction Limits of Nonadiabatic Strained Flames Against a Catalytic Surface, Fortieth AIAA Aerospace Sciences Meeting (AIAA Paper #2002-0621), Reno, NV, 2002.

S. B. Margolis and T. J. Gardner, Multiple Solutions, Extinction and Stability of Nonadiabatic Catalytic Flames in Stagnation-Point Flow, Ninth International Congress on Numerical Combustion, Sorrento, Italy, 2002.

S. B. Margolis and T. J. Gardner, Structure and Stability of Nonadiabatic Catalytic Flames in Stagnation-Point Flow, Forty-First AIAA Aerospace Sciences Meeting (AIAA Paper #2003-0669), Reno, NV, 2003.

References

[1] R. Srinivasan, I-M Hsing, J. Ryley, M.P. Harold, K.F. Jensen, and M.A. Schmidt, Micromachined chemical reactors for surface catalyzed oxidation reactions, *Tech. Digest 1996 Sol.-State Sensor and Actuator Workshop*, Transducers Research Foundation, Cleveland (1996) 15-18.

[2] L. R. Arana, S.B. Schaevitz, A.J. Franz, K.F. Jensen and M.A. Schmidt, A microfabricated suspended-tube chemical reactor for fuel processing, MEMS 2002, Las Vegas, NV, 1/20-24/2002, 232-235.

[3] M. Gall, The Si-planar-pellistor array, a detection unit for combustible gases, *Sensors and Actuators B*, 15-16 (1993) 260-264.

[4] R.P. Manginell, J.H. Smith, A.J. Ricco, D.J. Moreno, R.C. Hughes, R.J. Huber and S.D. Senturia, Selective, pulsed CVD of platinum on microfilament gas sensors, *Tech. Digest 1996 Sol.-State Sensor and Actuator Workshop*, Transducers Research Foundation, Cleveland (1996) 23-27.

[5] R.E.Cavicchi, J.S. Suehle, P. Chaparala, K.G. Kreider, M. Gaitan, and S. Semancik, Micro-hotplate gas sensor, *Tech. Digest 1994 Sol.-State Sensor and Actuator Workshop*, Cleveland (1994) 53-56.

[6] M.Zanini, J.H.Visser,L.Rimai,R.E.Soltis, A.Kovalchuk,D.W.Hoffmann, E.M. Logothetis, U. Bonne, L. Brewer, O.W. Byrnum, M.A. Richard, Fabrication and properties of a Si-based high sensitivity microcalorimetric gas sensor, *Tech. Digest 1994 Sol.-State Sensor and Actuator Workshop*, Cleveland (1994) 176-179.

[7] T. Holm, Aspects of the mechanism of the flame ionization detector, J. Chromatography A, 842 (1999) 221-227.

[8] S. Zimmermann, S. Wischhusen, J. Muller, Micro flame ionization detector and micro flame spectrometer, *Sensors And Actuators B,* 63 (2000) 159-166.

[9] R.P. Manginell, J.H. Smith, A.J. Ricco, R.J. Huber, R.C. Hughes, and D.J. Moreno, In-Situ Monitoring of Micro-Chemical Vapor Deposition (μ-CVD): Experimental Results and SPICE Modeling, *Tech. Digest 1998 Sol.-State Sensor and Actuator Workshop*, Transducers Research Foundation, Cleveland (1998) 371-374.

[10] G.B. Hocker, R.G. Johnson, R.E. Higashi, P.J.Bohrer, A microtransducer for air flow and differential pressure sensing applications, Micromachining and Micropackaging of Transducers, (1985) 207-214.

[11] G. Wachutka, et. al., Analytical 2-D model of CMOS micromachined gas flow sensors, *Digest of Technical Papers*, Transducers '91.

[12] E.H. Klaassen, G.T.A. Kovaks, Integrated thermal conductivity vacuum sensor, *Tech. Digest 1996 Sol.-State Sensor and Actuator Workshop*, Transducers Research Foundation, Cleveland (1996) 249-252.

[13] C.H. Mastrangelo, R.S. Muller, *Proceedings of Transducers '91*, San Francisco, (1991) 245-248.

[14] R.A. Wood, Uncooled thermal imaging with monolithic silicon focal planes, *SPIE Proceedings*, 2020 (1993) 322-329.

[15] M.H. Unewisse, S.J. Passmore, K.C. Liddiard and R.J. Watson, Performance of uncooled semiconductor film bolometer infrared detectors, *SPIE Proceedings*, 2269 (1994) 43-52.

[16] G. Sberveglieri, Recent developments in semiconducting thin-film gas sensors, *Sensors and Actuators B*, 2*3* (1995) 103-109.

[17] This circuit operates from +15V to –5V and uses an analog devices MLT04 chip in a divider configuration; otherwise it is conceptually similar to that shown in R.P. Manginell, J.H. Smith, A.J. Ricco, D.J. Moreno, R.C. Hughes, R.J. Huber, Electro-thermal modeling of a microbridge gas sensor, SPIE's 1997 Symposium on Micromachining and Microfabrication, Austin, TX, Sept. 29-30, 1997. SPIE Vol. 3224, pp. 360-371.

[18] NG mix: 9% ethane, 6% propane, 7% methane, 5% nitrogen, 3% n-butane, 1% carbon dioxide, 0.5% helium, 3% isobutane, 1% isopentane, 1% n-pentane, balance methane.

[19] F. Menil, C. Lucat, H. Debeda, The thick film route to selective gas sensors, *Sensors and Actuators B*, 24-25 (1995) 415-20.

[20] G. Frye-Mason, R. Kottenstette, P. Lewis, E. Heller, R. Manginell, D. Adkins, G. Dulleck, D. Martinez, D. Sasaki, C. Mowry, C. Matzke, and L. Anderson, "Hand-Held Miniature Chemical Analysis System (µChemlab) For Detection Of Trace Concentrations Of Gas Phase Analytes", *Proceedings of the µ-TAS '00 Worksho*p, Enchede, Netherlands, 5/14-18/00.

[21] M.W. Moorman, R. P. Manginell, C. Colburn, D.L. Mowery-Evans, P.G. Clem, N.S. Bell, L.F. Anderson, Microcombustor array and micro-flame ionization detector for hydrocarbon detection, SPIE Micromachining and Microfabrication Conference Proceedings, Santa Clara, CA, 1/25-31/2003, to appear.

Distribution List

Number of Copies	Mail Stop	Name	Organization
1	0188	LDRD Office	1030
3	0603	Ron Manginell	1764
1	0603	Matthew Moorman	1764
1	0603	Sara Sokolowski	1764
1	0603	L. James Sanchez	1764
1	0603	Sherry Zmuda	1764
1	0612	Review and Approval for DOE/OSTI	9612
1	0892	Chris Colburn	1764
1	0892	Larry Anderson	1764
1	0892	Richard Cernosek	1764
1	0892	Pat Lewis	1764
1	0892	Richard Kottenstette	1764
2	0899	Technical Library	9616
1	0959	Tim Gardner	14192
1	1349	Debbie Mowery-Evans	1846
1	1411	Paul Clem	1851
1	1425	Steve Martin	1707
1	9018	Central Technical Files	8945-1
1	9052	Steve Margolis	8361